Letter

Interlayer magnetoelectric coupling in van der Waals structures

Shiqiang Yu, Yushuo Xu, Ying Dai,* Dongyue Sun, Baibiao Huang, and Wei Wei†
School of Physics, State Key Laboratory of Crystal Materials, Shandong University, Jinan 250100, China

(Received 3 December 2023; accepted 23 February 2024; published 11 March 2024)

We propose a method to intrinsically realize the nonvolatile electrical control of noncollinear antiferromagnetism, and translate our idea to concrete van der Waals VI_2 bilayers from the first-principles calculations. In VI_2 bilayer systems, we unravel that the sliding ferroelectricity couples strongly to the spin spiral chirality of each VI_2 monolayer, which we refer to as the spin spiral chirality–sliding ferroelectricity locking effect. In this view, a flexibly electrical switch of the noncollinear antiferromagnetism can be realized via interlayer sliding. Our work therefore opens a different direction for the study of type-II multiferroic materials in two dimensions.

DOI: 10.1103/PhysRevB.109.L100402

In recent years, a growing interest has been raised in magnetoelectric multiferroics in two-dimensional (2D) materials, which combine magnetism and electric polarization and present great significance in fundamental magnetoelectric physics [1–4]. In light of the inherent repulsion between ferroelectricity and magnetism, electric polarization and magnetic moment usually originate from different sources, thus characterized by week magnetoelectric coupling and referred to as type-I multiferroics [5–8]. In order to advance the investigations in the field of magnetoelectric physics, type-II multiferroics with inherent magnetoelectric coupling has always been highly demanded. In a recent inspirational work, ferromagnetic VSe_2 monolayer was demonstrated to be a typical 2D type-II magnetoelectric multiferroics [9]. In particular, the coexistence and coupling of three ferroics in VSe_2 monolayer were revealed, that is, the ferromagnetism, spin-direction-dependent ferroelectricity, and ferrovalley. It was highlighted that the strong magnetoelectric coupling in 2D VSe_2 can enable the cross control of ferroic order parameters by external fields.

It is of high interest that noncollinear antiferromagnetic (AFM) order in 2D triangular lattices provides a straightforward way to obtain type-II magnetoelectric multiferroics [10–12]. In such a lattice, noncollinear spin spiral order due to the magnetic exchange frustration simultaneously breaks the spatial inversion symmetry and the time-reversal symmetry, triggering nondisplacive dipole moment and nonlinear interaction between magnetism and electric polarization [13,14]. In addition, noncollinear magnetic order endows 2D materials with a different quantum state, i.e., the spin spiral chirality that is in close relation with anomalous Hall conductivity [15,16]. In this view, effective control of the spin spiral chirality is of paramount importance to the applications of the noncollinear AFM materials. In previous investigations, various strategies have been implemented for modulating the noncollinear AFM state, such as applying magnetic field or spin-orbit torque induced by an electric current [17–19]. Nevertheless, these approaches are plagued by volatility, high energy consumption, and operational complexity. In this context, we propose a different approach beyond the current paradigm to realize nonvolatile electrical control of noncollinear magnetism, which will open a possibility for the development of high-performance, highly integrated magnetoelectric devices based on 2D noncollinear AFM materials.

In this work, we elucidate that interlayer sliding ferroelectricity can be considered to intrinsically achieve the nonvolatile electrical control of the noncollinear 120 °-ordered AFM (*Y*-AFM) state, and we demonstrate its feasibility in bilayer and trilayer VI_2. In particular, the in-plane spin spiral order in VI_2 monolayer can induce an interlocked out-of-plane ferroelectricity. In multilayer VI_2, robust sliding ferroelectricity can switch the spin spiral order induced ferroelectricity and thus the spin spiral chirality, which is referred to as the spin spiral chirality–sliding ferroelectricity locking effect. In such a way, nonvolatile electrical control of the noncollinear AFM state can be achieved. It should be pointed out that, additionally, the electric polarization in multilayer VI_2 is one order of magnitude larger than the spin spiral order induced electric polarization in the monolayer case. This makes the material more practical in experiments.

In 2D materials of triangular lattice, the noncollinear spin spiral order of an in-plane Y-AFM state can induce ferroelectricity, following the antisymmetric extended spin-current model $\boldsymbol{P} \propto \boldsymbol{S}_a \times \boldsymbol{S}_b$ [13,14]. It is evident that the spin spiral chirality can be manipulated by an external electric field, thereby achieving electrically controlled noncollinear magnetism. It has indeed been observed in previous work in multiferroic bulk $MnWO_4$ through polarization neutron diffraction [20]. In 2D form, however, nonvolatile electrically controlled noncollinear magnetism has never been realized because of the complex experiment procedure, small electric polarization, and low critical temperature.

In case two identical nonpolarized monolayers are stacked in a specific configuration forming the van der Waals bilayer; interlayer electric polarization emerges and can be reversed through interlayer sliding. It is referred to as sliding

*Corresponding author: daiy60@sdu.edu.cn
†Corresponding author: weiw@sdu.edu.cn

ferroelectricity, which has been proved in bilayers such as graphene [21], *h*-BN [22], $1T' - ReS_2$ [23], and $1T' - WTe_2$ [24]. In this regard, therefore, we expect to achieve the electrical control of noncollinear magnetism by sliding ferroelectricity rather than an external electric field.

In respect to a bilayer composed of two triangular lattices with in-plane *Y*-AFM state and corresponding out-of-plane spin spiral order induced electric polarization, specific stackings can generate a pair of opposite, reversible interlayer ferroelectric states. In *AA* stacking, interlayer electric polarization is absent and the bilayer is featured by two energetically degenerate *Y*-AFM ground states with the spin spiral chirality simultaneously pointing upwards or downwards. In this case we convert *AA* stacking to *AB* stacking through interlayer sliding, which exhibits an out-of-plane sliding ferroelectricity; a unique *Y*-AFM ground state with the spin spiral chirality in both monolayers in the same direction as the sliding induced electric field can be anticipated. In an alternative way, *AB*′ stacking can be attained. Without the consideration of *Y*-AFM order, *AB*′ stacking is energetically degenerate with *AB* stacking with however an opposite interlayer electric polarization. As magnetism is included, the magnetic ground state of *AB*′ stacking transitions to a noncollinear *Y*-AFM state with the spin spiral chirality in each monolayer parallel to the interlayer electric field. In other words, *AB* and *AB*′ stackings lift the degeneracy of the magnetic ground states in *AA* stacking, and the spin spiral chirality can be flexibly switched by interlayer sliding induced ferroelectricity, realizing the nonvolatile electrical control of magnetism. In this work, we refer to this phenomenon as a locking effect between spin spiral chirality and sliding ferroelectricity.

In the following, we translate our idea to a concrete material, i.e., VI_2. In Fig. 1(a), *T*-phase VI_2 monolayer of triangular lattice with a space group of $P\bar{3}m1$ is presented. In order to verify the magnetic ground state of VI_2 monolayer, collinear ferromagnetic (FM), ferrimagnetic (FiM), stripe AFM (*S*-AFM), and noncollinear *Y*-AFM orders are considered; see Fig. S1 of the Supplemental Material [25] and Figs. 1(b) and 1(c). In Table S1 of the Supplemental Material [25], results elucidate that the magnetic ground state is the *Y*-AFM order, consistent with previous experimental observations in bulk and monolayer VI_2 [26–28]. It should be kept in mind that VI_2 monolayer with *Y*-AFM order naturally has two energetically degenerate ground states with opposite spin spiral chirality, as depicted in Figs. 1(b) and 1(c). In the light of the same magnetic space group and crystal symmetry, two states show identical electronic properties.

It should be emphasized that the noncollinear spin spiral order in 2D triangular lattice provides two additional degrees of freedom, namely, the vector-spin spiral chirality [29,30],

$$\boldsymbol{V} = \frac{2}{3\sqrt{3}}(\hat{\boldsymbol{S}}_1 \times \hat{\boldsymbol{S}}_2 + \hat{\boldsymbol{S}}_2 \times \hat{\boldsymbol{S}}_3 + \hat{\boldsymbol{S}}_3 \times \hat{\boldsymbol{S}}_1)_z,$$

and the scalar-spin spiral chirality [31,32],

$$S = \hat{\boldsymbol{S}}_1 \cdot (\hat{\boldsymbol{S}}_2 \times \hat{\boldsymbol{S}}_3),$$

with $\boldsymbol{S}_{1,2,3}$ standing for the nearest-neighbor spins in a magnetic unit cell. In particular, $\boldsymbol{V}$ and S can be used to describe the coplanar and noncoplanar noncollinear magnets [33]. It is

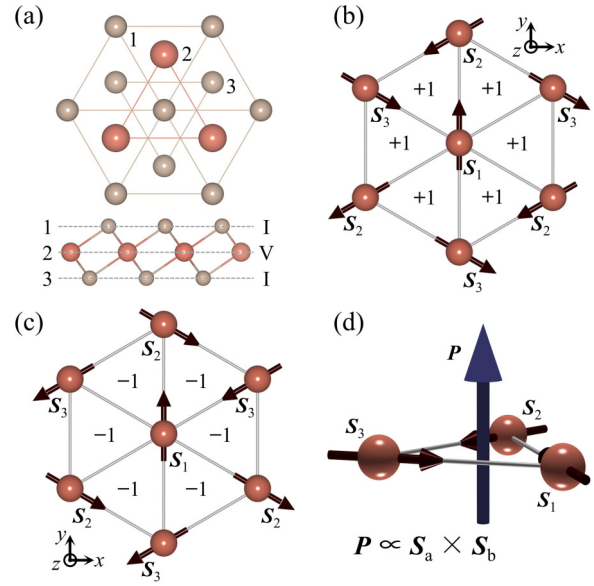

FIG. 1. (a) Top and side views of VI_2 monolayer. Orange and grey spheres symbolize V and I atoms, respectively. Noncollinear *Y*-AFM order in VI_2 monolayer with (b) positive ($V = +1$) and (c) negative ($V = -1$) spin spiral chirality. (d) Schematic of the spin spiral order induced electric polarization.

obvious that, in VI_2 monolayer, the scalar-spin spiral chirality S turns out to be zero due to the coplanar noncollinear *Y*-AFM ground state. In the case for the vector-spin spiral chirality for VI_2 monolayer in the in-plane *Y*-AFM state, $\boldsymbol{V}$ can be positive ($\boldsymbol{V} = +1$) and negative ($\boldsymbol{V} = -1$), corresponding to spin spiral chirality in the $+z$ and $-z$ directions, respectively. In Figs. 1(b) and 1(c), such a definition of the spin spiral chirality in VI_2 monolayer is illustrated, which is similar to the experimentally confirmed AFM kagome lattice with $q = 0$ structure [30].

In accordance to the generalized spin-current model [13,14], spin spiral order of VI_2 monolayer can induce a nondisplacive ferroelectricity,

$$\boldsymbol{P} = \mathbf{M} \sum_{\langle ij \rangle} (\boldsymbol{S}_i \times \boldsymbol{S}_j),$$

where S denotes spin vector, i, j represents spin components, the summation is over all the nearest-neighbor bonds, and $\mathbf{M}$ corresponds to a 3×3 coefficient matrix. In particular, our first-principles calculation finds

$$M = -\begin{pmatrix} 3.89 & 0 & 0 \\ 0 & 3.89 & 0 \\ 0 & 0 & 1.96 \end{pmatrix} \times 10^{-3}\,\mathrm{e\,\AA}.$$

It reveals that the spin spiral order induced ferroelectricity in VI_2 monolayer follows an antisymmetric mechanism $\boldsymbol{P} \propto \boldsymbol{S}_\mathrm{i} \times \boldsymbol{S}_\mathrm{j}$, and the electric polarization is interlocked with the spin spiral chirality, as shown in Fig. 1(d). In general, the spin-induced polarization can be described by a common spin-current mechanism $\boldsymbol{P} \propto \boldsymbol{e}_\mathrm{ij} \times (\boldsymbol{S}_\mathrm{i} \times \boldsymbol{S}_\mathrm{j})$, where $\boldsymbol{e}_\mathrm{ij}$ is the unit vector connecting the spin pairs. In this case, the coefficient matrix $\mathbf{M}$ should present nonzero off-diagonal matrix elements [14]. In Fig. S2 [25], for a clear expression of this

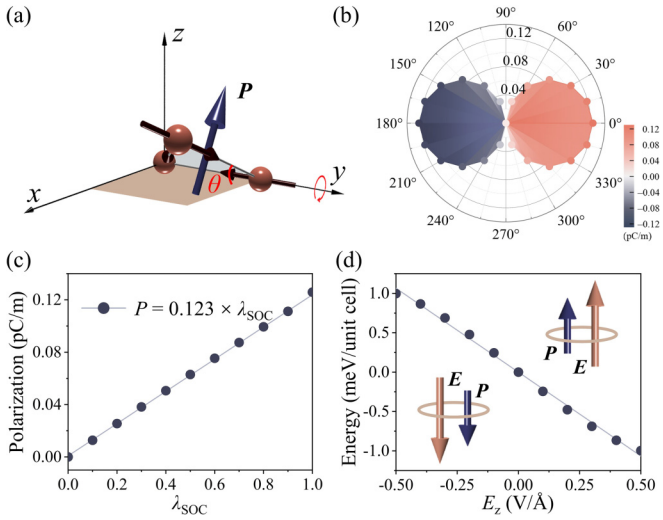

FIG. 2. (a) Schematic of the spin spiral plane rotating around y axis. (b) Electric polarization of VI_2 monolayer in z direction as a function of rotation angle (θ). (c) Electric polarization as a function of SOC strength (λ_{SOC}). (d) Energy difference between two Y-AFM states with opposite spin spiral chirality caused by external electric field. Insets represent the coupling between the induced electric polarization and the vertical electric field.

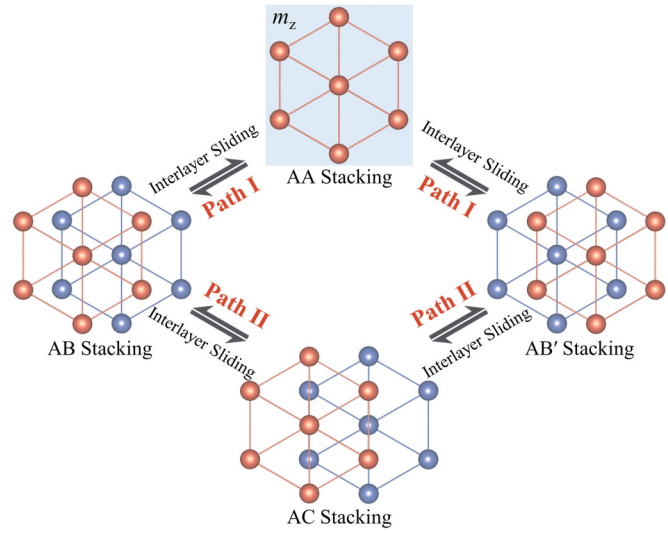

FIG. 3. AA, AB, AC, and AB' stackings and two interlayer sliding pathways from AB to AB' stacking. Orange and blue spheres denote V atoms in the upper and lower monolayer, respectively.

mechanism, a schematic for the local electric polarization of each type of bond and the total electric polarization of the Y-AFM state is provided. It can be concluded that, regardless of the direction of spin spiral chirality, spin-induced in-plane electric polarization following this mechanism is cancelled out in the sum of all spin pairs. In accordance with the antisymmetric mechanism $\boldsymbol{P} \propto \boldsymbol{S}_i \times \boldsymbol{S}_j$, then, the out-of-plane total electric polarization can be derived. In this context, coefficient matrix $\mathbf{M}$ only has nonzero diagonal matrix elements, which is consistent with the situation with a spiral wave vector of $q = 1/3$ [14]. In regard to the coplanar noncollinear Y-AFM ground state, therefore, the antisymmetric mechanism is applicable. In Fig. S3 [25], the band structure of VI_2 monolayer of the Y-AFM state indicates an indirect band gap of 2.23 eV, thus effectively avoiding the screening of the static internal field caused by the long-range dipole moment of conducting electrons.

In respect to a noncollinear Y-AFM order, identifying its easy plane is crucial as it determines the direction of the induced electric polarization. In the case of VI_2 monolayer, the total energy of in-plane (ab) Y-AFM order is 0.08 meV/unit cell lower than that in the ac/bc plane, indicative of a spin spiral chirality perpendicular to the ab plane. It can be found that the z-direction electric polarization shows a cosine modulation of the rotation angle θ, suggesting a robust dependence; see Figs. 2(a) and 2(b). In particular, as $\theta = 0\,^\circ$, VI_2 monolayer corresponds to an in-plane Y-AFM state with an out-of-plane electric polarization of 0.12 pC/m, while at $\theta = 180\,^\circ$ the electric polarization as well as the spin spiral chirality reverse. In the present work, we emphasize that VI_2 monolayer is an extremely rare case with the induced ferroelectricity being out of plane. It should be pointed out that spin-orbit coupling (SOC) plays a crucial role in the magnetoelectric coupling in VI_2. It can be found from Fig. 2(c) that the electric polarization presents a perfect linear relationship with the SOC strength (with the coefficient of determination being 0.99). In the case of $\lambda_{SOC} = 0$, spin spiral order induced electric polarization vanishes. It therefore can be concluded that, in regard to VI_2 monolayer, the in-plane spin spiral order in combination with SOC induces the out-of-plane ferroelectricity.

In Fig. 2(d), the effect of an external electric field on the spin spiral chirality can be observed. That is, the field can lift the degeneracy of two Y-AFM states with opposite spin spiral chirality. In the case of applying a field of 0.5 V/Å, for example, the energy difference between two Y-AFM states achieves 0.99 meV/unit cell. In particular, the direction of the spin spiral chirality can be tuned to the same direction as the field. It therefore is compelling evidence for the realization of electrical control of noncollinear magnetism by interlayer sliding ferroelectricity in VI_2 bilayer.

In VI_2 bilayer, the upper layer can be obtained by an operation of $t_z R t_0$ to the lower layer, with t_z, R, and t_0 being the out-of-plane translation, rotation, and in-plane translation, respectively. In the case that VI_2 bilayer has the same unit cell size as that of the constituting monolayer, R must be a symmetric operation belonging to the point group G_L of its 2D Bravais lattice. In consideration that R is equivalent to RP_m (P_m is the symmetric operation of the point group G_M of VI_2 monolayer), R turns out to be an element of the factor group $G_R = \frac{G_L}{G_M} = \frac{D_{6h}}{D_{3d}} = \{E, m_z\}$. When $R = E$, the as-formed VI_2 bilayers present inversion symmetry, and, therefore, out-of-plane electric polarization is forbidden [34]. As $R = m_z$, operation $t_z m_z t_0$ generates VI_2 bilayers with broken inversion symmetry, thus providing the possibility of an out-of-plane electric polarization.

In Fig. 3, AA, AB, and AB' stackings under different t_0 are shown. In particular, $t_0 = (0, 0, 0)$ raises the VI_2 bilayer in AA stacking (D_{3h}) with a mirror symmetry m_z, which presents, however, no out-of-plane electric polarization. $t_0 = (1/3, -1/3, 0)/(1/3, 2/3, 0)/(-2/3, -1/3, 0)$ and $t_0 = (2/3, 1/3, 0)/(-1/3, 1/3, 0)/(-1/3, -2/3, 0)$ can transfer

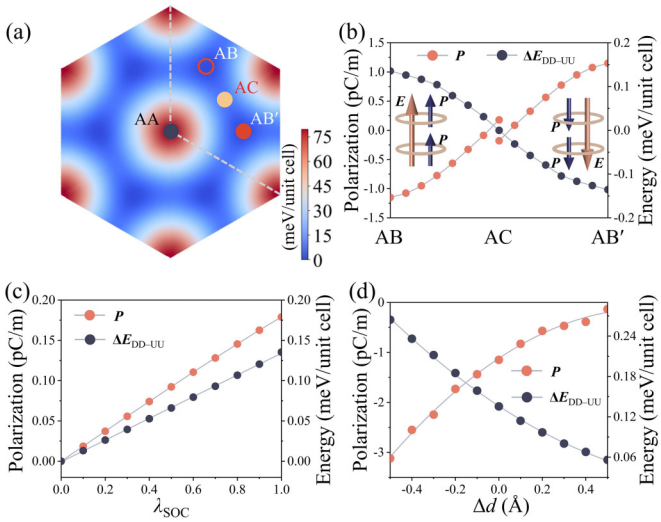

FIG. 4. (a) Energy distribution for different bilayer stacking styles, with the total energy of *AB* stacking as a reference. (b) Variations of electric polarization and $\Delta E_{\mathrm{DD-UU}}$ as $AB \rightarrow AB'$. Insets show the spin spiral chirality–sliding ferroelectricity locking effect. (c) Spin spiral order induced electric polarization and $\Delta E_{\mathrm{DD-UU}}$ as a function of SOC strength (λ_{SOC}) in *AB* stacking. (d) Electric polarization and $\Delta E_{\mathrm{DD-UU}}$ as a function of interlayer distance change (Δd).

AA stacking to energetically degenerate *AB* and *AB*′ stackings (C_{3v}), respectively. In *AB* and *AB*′ stackings, out-of-plane electric polarization emerges in opposite directions, representing a pair of ferroelectric configurations that can be flexibly switched through interlayer sliding. Based on the Berry phase method, the out-of-plane sliding ferroelectricity of *AB*/*AB*′ stacking is calculated to be −1.33/1.33 pC/m (without considering the *Y*-AFM state). It should be emphasized that such an electric polarization is even larger than that of $1T' - ReS_2$ bilayer (0.07 pC/m) [23], $1T' - WTe_2$ bilayer (0.38 pC/m) [24], and VSi_2P_4 bilayer (0.42 pC/m) [35], underscoring the experimental accessibility of the electric polarization of VI_2 bilayer. In comparison to monolayer, the sliding electric polarization is one order of magnitude larger than the spin spiral order induced electric polarization, therefore making the system more practical in applications.

In Fig. S4 [25], two sliding pathways switching the *AB* and *AB*′ stackings are shown. In the case of path I, $AB \rightarrow AB'$ occurs as $t_0 = (-2/3, -4/3, 0)/(-2/3, 2/3, 0)/(4/3, 2/3, 0)$, with *AA* stacking being the transition state. In regard to path II, $t_0 = (1/3, 2/3, 0)/(1/3, -1/3, 0)/(-2/3, -1/3, 0)$ causes the $AB \rightarrow AB'$ switch, with a transition state of *AC* stacking. In Fig. S5 [25], band structures of *AA*, *AB*, *AB*′, and *AC* stackings are shown. It can be seen that *AB* and *AB*′ stackings exhibit opposite band offset due to the inversion of the interlayer electric polarization, while the band offset in unpolarized *AA* and *AC* stackings is negligible. In two pathways, *AB* and *AB*′ stackings are the most stable configurations; see Fig. 4(a). The energy barrier along path II is significantly lower than that of path I, 21.06 vs 77.52 meV/unit cell, which is also lower than that of Sb bilayer (38 meV/unit cell) [36] while larger than those of *h*-BN bilayer (4.5 meV/unit cell) [37] and VSe_2 bilayer (20 meV/unit cell) [38]. Generally, the energy barrier should be neither too large nor too small; such a moderate energy barrier is in favor of the easy ferroelectricity switching between *AB* and AB′ stackings.

To determine the ground state of VI_2 bilayer, magnetic configurations including interlayer collinear FM and AFM states, and noncollinear *Y*-AFM states with the spin spiral chirality of each layer pointing upwards (UU), downwards (DD), and in opposite directions (head-to-head order as DU and tail-to-tail order as UD) are taken into account. In Table S2 [25], the total energies of *AB*, *AB*′, and *AC* stackings with six magnetic orders of consideration are summarized. It can be found that the magnetic ground state of VI_2 bilayer features a noncollinear *Y*-AFM state with the direction of the spin spiral chirality in both monolayers aligned with interlayer electric field. This is an important result for the following discussion.

In Fig. 4(b), variations of the electric polarization and energy difference $\Delta E_{\mathrm{DD-UU}}$ during the sliding along path II are shown. It can be found that a spin spiral order induced electric polarization of 0.18 pC/m exists in *AC* stacking, causing a discontinuity at the *AC* point. In *AB* or *AB*′ stacking with noncollinear *Y*-AFM ground state considered, the net out-of-plane electric polarization is 1.15 pC/m. It is of paramount importance that the energy degeneracy of *AB* and *AB*′ stackings are lifted when the *Y*-AFM order is included, and $|\Delta E_{\mathrm{DD-UU}}|$ reaches 0.14 meV/unit cell. It indicates that, therefore, the spin spiral chirality can be effectively modulated by the sliding ferroelectricity. This confirms the feasibility of our proposed method to realize the electrical control of noncollinear magnetism.

Taking *AB* stacking as a representative, the coupling between spin spiral order induced ferroelectricity and sliding electric polarization is validated through the control of λ_{SOC}. It can be found from Fig. 4(c) that the spin spiral order induced polarization increases linearly as λ_{SOC} increases, and as well as the $\Delta E_{\mathrm{DD-UU}}$. When λ_{SOC} is zero, spin spiral order induced ferroelectricity disappears while sliding ferroelectricity exists. In this case, however, *AB* stacking presents two degenerate noncollinear *Y*-AFM states with opposite spin spiral chirality. These results therefore confirm the coupling between two kinds of ferroelectricity and support our proposed method for electrically controlled magnetism in triangular-lattice antiferromagnets.

In van der Waals bilayers, interlayer distance is a significant ingredient influencing the magnetoelectric coupling. In addition, strategies for controlling the interlayer distance have been proposed, for instance, through introducing active sites [39], controlling the saturation vapor pressure of adsorbed water molecules [40], and physical compression as well [41,42]. It can be observed from Fig. 4(d), that, taking *AB* stacking as a representative, the out-of-plane electric polarization increases as the interlayer distance decreases, as well as the $\Delta E_{\mathrm{DD-UU}}$ compared to the case at equilibrium interlayer distance. In particular, the electric polarization and $\Delta E_{\mathrm{DD-UU}}$ turn out to be 3.12 pC/m and 0.26 meV, respectively, as the interlayer distance decreases by 0.5 Å. In the case where the interlayer distance is decreased by 1.0 Å, the electric polarization (–7.09 pC/m) and $\Delta E_{\mathrm{DD-UU}}$ (0.40 meV/unit cell) can be increased further; see Fig. S6 [25]. It can be concluded that, therefore, vertical compressive strain can effectively enhance the

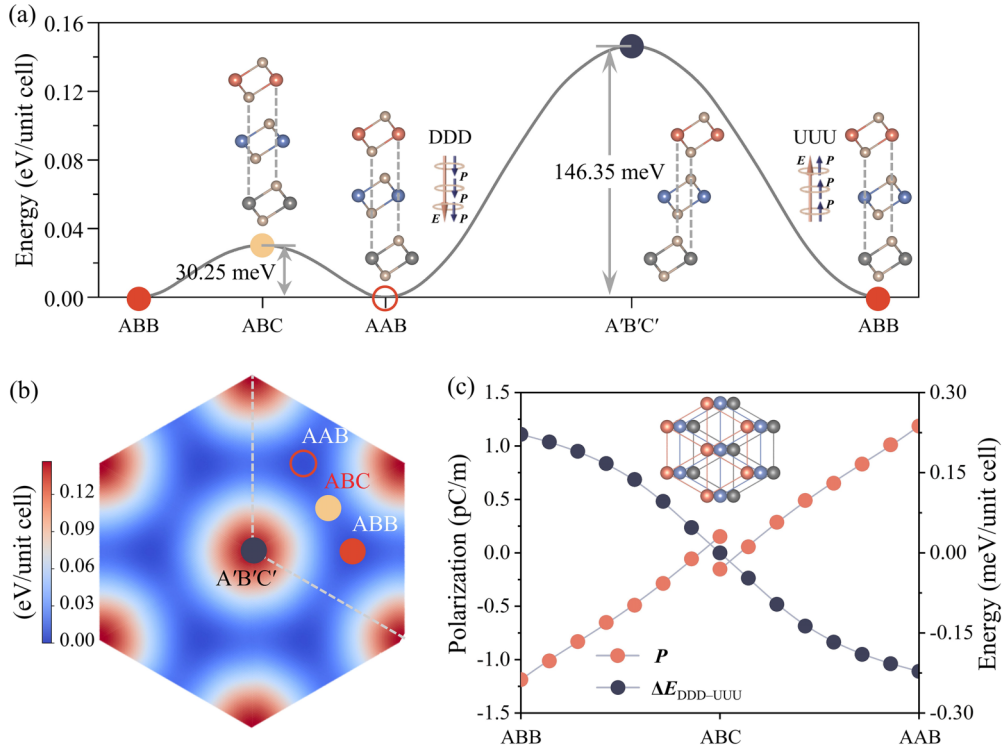

FIG. 5. (a) Energy profile for *ABB* → *AAB* → *ABB* interlayer sliding; corresponding stackings are also shown. (b) Energy distribution for different trilayer stacking styles, with the total energy of *AAB* stacking as a reference. (c) Electric polarization and $\Delta E_{\mathrm{DDD-UUU}}$ during the interlayer sliding from *ABB* to *AAB* stacking. Inset shows the top view of *ABC* stacking.

coupling between spin spiral order induced ferroelectricity and the sliding ferroelectricity in VI_2 bilayers.

In light of strong the magnetoelectric coupling in VI_2, it can be expected that applying a vertical electric field can increase the energy difference $\Delta E_{\mathrm{DD-UU}}$. It can be seen from Fig. S7 [25] that, taking *AB* stacking as a representative, an external electric field further lifts the degeneracy of two noncollinear *Y*-AFM states, with $\Delta E_{\mathrm{DD-UU}}$ reaching 0.31 meV/unit cell under a field of 0.05 V/Å. It is therefore also an effective way to obtain the more stable noncollinear magnetic ground state of VI_2 bilayer.

Our mechanism for electrical control of noncollinear magnetism is also applicable in VI_2 trilayers. As shown in Fig. S8 [25], *AAA* stacking with a point group of D_{3d} can be transferred to *AAB* and *ABB* stackings (C_{3v}), which bear out-of-plane electric polarization in opposite directions. In Fig. S9 [25], two sliding paths (I and II) from *AAB* stacking to *ABB* stacking through in-plane translation are illustrated. Along path I and path II, the transition states correspond respectively to $A'B'C'$ stacking (D_{3d}) and *ABC* stacking (C_s), both of which exhibit no out-of-plane electric polarization. As shown in Fig. 5(a), path II is more preferable (an energy barrier of 146.35 meV/unit cell for path I and 30.25 meV/unit cell for path II). We can see from Fig. 5(b) that *AAB* and *ABB* stackings are the most stable configurations. In Fig. 5(c), variations of the out-of-plane electric polarization and energy difference $\Delta E_{\mathrm{DDD-UUU}}$ during the sliding from *ABB* stacking to *AAB* stacking along path II are illustrated. It can be known that the spin spiral chirality of *AAB* stacking tends to be a *DDD* order because of the upward sliding electric polarization, while the *UUU* order of the spin spiral chirality is stable in *ABB* stacking. In particular, $|\Delta E_{\mathrm{DDD-UUU}}|$ can reaches a maximum value of 0.22 meV/unit cell in *AAB*/*ABB* stacking with an out-of-plane electric polarization of 1.19 pC/m. In *ABC* stacking, such two noncollinear magnetic states (*DDD* and *UUU*) are energetically degenerate. It therefore can be concluded that electrical control of noncollinear magnetism can also be realized in multilayer cases.

In analogy to VI_2 bilayer, vertical external electric field and decreased interlayer distance can improve the energy difference $|\Delta E_{\mathrm{DDD-UUU}}|$ in VI_2 trilayer; see Figs. S6 and S7 [25]. In the case of *ABB* stacking, for instance, the electric polarization and $|\Delta E_{\mathrm{DDD-UUU}}|$ increase to 10.24 pC/m and 0.85 meV/unit cell, respectively, as the interlayer distance is decreased by 1.0 Å. In addition, $|\Delta E_{\mathrm{DDD-UUU}}|$ can increase to 0.57 meV/unit cell under an external electric field of 0.05 V/Å. It therefore can be concluded that both external electric field and decreased interlayer distance can enhance the interlayer magnetoelectric coupling and stabilize the ground state.

In summary, we propose that the noncollinear AFM state can be controlled by sliding ferroelectricity and prove it in multilayer VI_2. In VI_2 monolayer, the spin spiral chirality is interlocked with the induced electric polarization, and, therefore, is switchable by an external electric field. In cases for VI_2 multilayers, the electric polarization is one order of magnitude larger than that of the monolayer case, making the systems more practical in applications. We confirm that the sliding ferroelectricity can replace external field to flexibly control the spin spiral order induced electric polarization and

the corresponding spin spiral chirality, termed as spin spiral chirality–sliding ferroelectricity locking effect. Our work opens an avenue for realizing the nonvolatile electrical control of noncollinear magnetism, which is expected to interest the experimentalists.

This work was supported by the National Natural Science Foundation of China (Grants No. 52272223 and No. 12074217) and the Shandong Provincial Key Research and Development Program (the Major Scientific and Technological Innovation Project) (Project No. 2019JZZY010302).

[1] Q. Song, C. A. Occhialini, E. Ergeçen, B. Ilyas, D. Amoroso, P. Barone, J. Kapeghian, K. Watanabe, T. Taniguchi, A. S. Botana, S. Picozzi, N. Gedik, and R. Comin, Evidence for a single-layer van der Waals multiferroic, Nature (London) **602**, 601 (2022).

[2] C. Zhang, P. Guo, and J. Zhou, Tailoring bulk photovoltaic effects in magnetic sliding ferroelectric materials, Nano Lett. **22**, 9297 (2022).

[3] M. Xu, C. Huang, Y. Li, S. Liu, X. Zhong, P. Jena, E. Kan, and Y. Wang, Electrical control of magnetic phase transition in a type-I multiferroic double-metal trihalide monolayer, Phys. Rev. Lett. **124**, 067602 (2020).

[4] H. Ai, F. Li, H. Bai, D. Liu, K. Ho Lo, S. A. Yang, Y. Kawazoe, and H. Pan, Ferroelectricity coexisted with *p*-orbital ferromagnetism and metallicity in two-dimensional metal oxynitrides, npj Comput. Mater. **8**, 60 (2022).

[5] W. Luo, K. Xu, and H. Xiang, Two-dimensional hyperferroelectric metals: A different route to ferromagnetic-ferroelectric multiferroics, Phys. Rev. B **96**, 235415 (2017).

[6] S. Yu, Y. Wang, S. Wang, H. Zhang, B. Huang, Y. Dai, and W. Wei, Robust intrinsic multiferroicity in a $FeHfSe_3$ layer, J. Phys. Chem. Lett. **12**, 8882 (2021).

[7] Y. Lai, Z. Song, Y. Wan, M. Xue, C. Wang, Y. Ye, L. Dai, Z. Zhang, W. Yang, H. Du, and J. Yang, Two-dimensional ferromagnetism and driven ferroelectricity in van der Waals $CuCrP_2S_6$, Nanoscale **11**, 5163 (2019).

[8] T. H. X. Tan, M. L. Li, H. T. Liu, Z. R. Liu, Y. C. Li, and W. H. Duan, Two-dimensional ferromagnetic-ferroelectric multiferroics in violation of the d^0 rule, Phys. Rev. B **99**, 195434 (2019).

[9] F. Wang, Y. Zhou, X. Shen, S. Dong, and J. Zhang, Magnetoelectric coupling and cross control in two-dimensional ferromagnets, Phys. Rev. Appl. **20**, 064011 (2023).

[10] J. J. Zhang, L. Lin, Y. Zhang, M. Wu, B. I. Yakobson, and S. Dong, Type-II multiferroic $Hf_2VC_2F_2$ MXene monolayer with high transition temperature, J. Am. Chem. Soc. **140**, 9768 (2018).

[11] D.-L. Bao, A. O'Hara, S. Du, and S. T. Pantelides, Tunable, ferroelectricity-inducing, spin-spiral magnetic ordering in monolayer FeOCl, Nano Lett. **22**, 3598 (2022).

[12] A. O. Fumega and J. L. Lado, Microscopic origin of multiferroic order in monolayer NiI_2, 2D Mater. **9**, 025010 (2022).

[13] H. J. Xiang, E. J. Kan, Y. Zhang, M. H. Whangbo, and X. G. Gong, General theory for the ferroelectric polarization induced by spin-spiral order, Phys. Rev. Lett. **107**, 157202 (2011).

[14] J. T. Zhang, C. Ji, J. L. Wang, W. S. Xia, B. X. Guo, X. M. Lu, and J. S. Zhu, Spin-induced ferroelectricity in a triangular-lattice antiferromagnet studied by magnetoelectric coupling tensors, Phys. Rev. B **96**, 235136 (2017).

[15] S. Hu, D.-F. Shao, H. Yang, C. Pan, Z. Fu, M. Tang, Y. Yang, W. Fan, S. Zhou, E. Y. Tsymbal, and X. Qiu, Efficient perpendicular magnetization switching by a magnetic spin Hall effect in a noncollinear antiferromagnet, Nat. Commun. **13**, 4447 (2022).

[16] O. Busch, B. Göbel, and I. Mertig, Spin Hall effect in noncollinear kagome antiferromagnets, Phys. Rev. B **104**, 184423 (2021).

[17] P. Lukashev, R. F. Sabirianov, and K. Belashchenko, Theory of the piezomagnetic effect in Mn-based antiperovskites, Phys. Rev. B **78**, 184414 (2008).

[18] S. Nakatsuji, N. Kiyohara, and T. Higo, Large anomalous Hall effect in a non-collinear antiferromagnet at room temperature, Nature (London) **527**, 212 (2015).

[19] H. Tsai, T. Higo, K. Kondou, T. Nomoto, A. Sakai, A. Kobayashi, T. Nakano, K. Yakushiji, R. Arita, S. Miwa, Y. Otani, and S. NaKatsuji, Electrical manipulation of a topological antiferromagnetic state, Nature (London) **580**, 608 (2020).

[20] T. Finger, D. Senff, K. Schmalzl, W. Schmidt, L. P. Regnault, P. Becker, L. Bohatý, and M. Braden, Electric-field control of the chiral magnetism of multiferroic $MnWO_4$ as seen via polarized neutron diffraction, Phys. Rev. B **81**, 054430 (2010).

[21] L. Yang, S. Ding, J. Gao, and M. Wu, Atypical sliding and Moiré ferroelectricity in pure multilayer graphene, Phys. Rev. Lett. **131**, 096801 (2023).

[22] K. Yasuda, X. Wang, K. Watanabe, T. Taniguchi, and P. Jarillo-Herrero, Stacking-engineered ferroelectricity in bilayer boron nitride, Science **372**, 1458 (2021).

[23] Y. Wan, T. Hu, X. Mao, J. Fu, K. Yuan, Y. Song, X. Gan, X. Xu, M. Xue, X. Cheng, C. Huang, J. Yang, L. Dai, H. Zeng, and E. Kan, Room-temperature ferroelectricity in 1T'-ReS_2 multilayers, Phys. Rev. Lett. **128**, 067601 (2022).

[24] Z. Fei, W. Zhao, T.A. Palomaki, B. Sun, M.K. Miller, Z. Zhao, J. Yan, X. Xu, and D.H. Cobden, Ferroelectric switching of a two-dimensional metal, Nature (London) **560**, 336 (2018).

[25] See Supplemental Material at http://link.aps.org/supplemental/10.1103/PhysRevB.109.L100402 for (i) computational methods; (ii) possible magnetic states of VI_2 monolayer; (iii) total electric polarization in *Y*-AFM state with different spin spiral chirality; (iv) band structure of VI_2 monolayer with *Y*-AFM state; (v) total energies of monolayer and bilayer VI_2 with different magnetic states; (vi) band structure of VI_2 bilayer with different stacking patterns; (vii) interlayer sliding pathways for bilayer and trilayer VI_2; (viii) energy difference ($\Delta E_{\mathrm{DD-UU}}$ and $\Delta E_{\mathrm{DDD-UUU}}$) of bilayer and trilayer VI_2 with vertical external electric field and decreased interlayer distance.

[26] S. R. Kuindersma, C. Haas, J. P. Sanchez, and R. Al, Magnetic structures and properties of VI_2, Solid State Commun. **30**, 403 (1979).

[27] K. Hirakawa, H. Kadowaki, and K. Ubukoshi, Study of frustration effects in two-dimensional triangular lattice antiferromagnets–neutron powder diffraction study of VX_2, X ≡ Cl, Br and I, J. Phys. Soc. Jpn. **52**, 1814 (1983).

[28] X. Zhou, Z. Wang, H. Zhu, Z. Liu, Y. Hou, D. Guo, and D. Zhong, Epitaxial growth and electronic properties of an antiferromagnetic semiconducting VI_2 monolayer, Nanoscale **14**, 10559 (2022).

[29] D. Grohol, K. Matan, J.-H. Cho, S.-H. Lee, J. W. Lynn, D. G. Nocera, and Y. S. Lee, Spin chirality on a two-dimensional frustrated lattice, Nat. Mater. **4**, 323 (2005).

[30] T. Inami, M. Nishiyama, S. Maegawa, and Y. Oka, Magnetic structure of the *kagomé* lattice antiferromagnet potassium jarosite $KFe_3(OH)_6(SO_4)_2$, Phys. Rev. B **61**, 12181 (2000).

[31] R. Shindou and N. Nagaosa, Orbital ferromagnetism and anomalous Hall effect in antiferromagnets on the distorted fcc lattice, Phys. Rev. Lett. **87**, 116801 (2001).

[32] S. Grytsiuk, J.-P. Hanke, M. Hoffmann, J. Bouaziz, O. Gomonay, G. Bihlmayer, S. Lounis, Y. Mokrousov, and S. Blügel, Topological–chiral magnetic interactions driven by emergent orbital magnetism, Nat. Commun. **11**, 511 (2020).

[33] X. Zhou, W. Feng, Y. Li, and Y. Yao, Spin-chirality-driven quantum anomalous and quantum topological Hall effects in chiral magnets, Nano Lett. **23**, 5680 (2023).

[34] J. Ji, G. Yu, C. Xu, and H. J. Xiang, General theory for bilayer stacking ferroelectricity, Phys. Rev. Lett. **130**, 146801 (2023).

[35] T. Zhang, X. Xu, B. Huang, Y. Dai, L. Kou, and Y. Ma, Layer-polarized anomalous Hall effects in valleytronic van der Waals bilayers, Mater. Horiz. **10**, 483 (2023).

[36] Y. Liang, R. Guo, S. Shen, B. Huang, Y. Dai, and Y. Ma, Out-of-plane ferroelectricity and multiferroicity in elemental bilayer phosphorene, arsenene, and antimonene, Appl. Phys. Lett. **118**, 012905 (2021).

[37] L. Li and M. Wu, Binary compound bilayer and multilayer with vertical polarizations: Two-dimensional ferroelectrics, multiferroics, and nanogenerators, ACS Nano **11**, 6382 (2017).

[38] X. Liu, A. P. Pyatakov, and W. Ren, Magnetoelectric coupling in multiferroic bilayer VS_2, Phys. Rev. Lett. **125**, 247601 (2020).

[39] Y. Ding, M. Zeng, Q. Zheng, J. Zhang, D. Xu, W. Chen, C. Wang, S. Chen, Y. Xie, Y. Ding, S. Zheng, J. Zhao, P. Gao, and L. Fu, Bidirectional and reversible tuning of the interlayer spacing of two-dimensional materials, Nat. Commun. **12**, 5886 (2021).

[40] C. Liu, X. Zou, Y. Lv, X. Liu, C. Ma, K. Li, Y. Liu, Y. Chai, L. Liao, and J. He, Controllable van der Waals gaps by water adsorption, Nat. Nanotechnol. (2024), doi: 10.1038/s41565-023-01579-w.

[41] A. P. Nayak, S. Bhattacharyya, J. Zhu, J. Liu, X. Wu, T. Pandey, C. Q. Jin, A. K. Singh, D. Akinwande, and J. F. Lin, Pressure-induced semiconducting to metallic transition in multilayered molybdenum disulphide, Nat. Commun. **5**, 3731 (2014).

[42] J. Xia, J. Yan, Z. Wang, Y. He, Y. Gong, W. Chen, T. C. Sum, Z. Liu, P. M. Ajayan, and Z. Shen, Strong coupling and pressure engineering in WSe_2-MoSe_2 heterobilayers, Nat. Phys. **17**, 92 (2021).